Open-Ended, N-Doped Carbon Nanotube–Graphene Hybrid Nanostructures as High-Performance Catalyst Support

Ruitao Lv, Tongxiang Cui, Mun-Suk Jun, Qiang Zhang, Anyuan Cao, Dang Sheng Su, Zhengjun Zhang, Seong-Ho Yoon, Jin Miyawaki, Isao Mochida, and Feiyu Kang**

A hierarchical N-doped carbon nanotube-graphene hybrid nanostructure (NCNT-GHN), in which the graphene layers are distributed inside the CNT inner cavities, was designed to efficiently support noble metal (e.g., PtRu) nanoparticles. Well-dispersed PtRu nanoparticles with diameters of 2–4 nm were immobilized onto these NCNT-GHN supports by a low-temperature chemical reduction method without any pretreatment. Compared to conventional CNTs and commercial catalysts. a much better catalytic performance was achieved by a synergistic effect of the hierarchical structure (graphene-CNT hybrid) and electronic modulation (N-doping) during the methanol electrooxidation reaction. Improved single-cell performances with long-term stability are also demonstrated using NCNT-GHN as catalyst support.

1. Introduction

Platinum or Pt-based alloy nanoparticles exhibit a high catalytic activity for various chemical reactions and have been widely used in areas such as fuel cells,[1] solar cells,[2] heterogeneous catalysis,[3] magnetic recording media,[4] etc. However, because of the limited resources and high cost of platinum, the utilization efficiency of the noble metal must be improved because so far it has not been possible to fully replace Pt by other metals or alloys because of its unique and excellent catalytic performance.[5] The catalytic activity of the noble metal depends strongly on the shape, size, and distribution of the particles. An efficient way to achieve better utilization of Pt-based nanoparticles is to disperse them onto a suitable support, which should fulfill the following requirements: the support needs to have 1) a high surface area and strong affinity for the catalyst particles to ensure their efficient immobilization in a well-dispersed way, 2) a high electrical conductivity to facilitate fast electron transfer in many redox reactions, 3) an excellent chemical stability in the operating environment to maintain a stable catalyst structure.[6] Compared to the conventional carbon-black support, carbon nanotubes (CNTs) have been demonstrated as a kind of advanced support material for Pt and Pt-based nanoparticles, because of their large aspect ratio, high electrical conductivity, and good chemical stability.[7] Nevertheless, because of their surface inertness and thus insufficient anchoring sites for binding metal nanoparticles, the CNTs usually require a suitable surface functionalization pretreatment for better catalyst particle immobilization, such as acid oxidation,[7a–c] ionic liquid (IL) linking,[7d–f] polymer wrapping,[7g,h] plasma treatment,[7i] etc. However, these functionalization pretreatments might cause a partial destruction of the CNT structure leading to a decrease in its electrical conductivity,[7a–c,8] or require additional complicated procedures before metal nanoparticle immobilization.[7d–i] Therefore, it is crucial to develop a CNT-based support for high-efficiency immobilization of mono-dispersed Pt-based nanoparticles with high catalytic activity without the need for any pretreatment.

Heteroatom (e.g., nitrogen)-doped CNTs have been proven theoretically to be an excellent support for noble metal nanoparticles by enhancing the metal-CNT binding through the large electron affinity of nitrogen.[9] Previous experimental work has also demonstrated that the incorporation of nitrogen can enhance the chemical reactivity of CNTs, and is favorable for the nucleation of fine metal-catalyst particles.[7i,10] However, because of the small inner diameters (e.g., 6–8 nm[10]) and usually closed tips of nitrogen-doped CNTs (NCNTs) only the external surface of NCNTs can be utilized

Dr. R. T. Lv, T. X. Cui, Prof. Z. J. Zhang, Prof. F. Y. Kang
Laboratory of Advanced Materials
Department of Materials Science and Engineering
Tsinghua University
Beijing 100084, P.R. China
E-mail: fykang@tsinghua.edu.cn
Dr. M. S. Jun, Prof. S. H. Yoon, Dr. J. Miyawaki, Prof. I. Mochida
Institute for Materials Chemistry and Engineering
Kyushu University
Kasuga, Fukuoka 816–8580, Japan
Dr. Q. Zhang, Prof. D. S. Su
Department of Inorganic Chemistry
Fritz Haber Institute of the Max Planck Society
Faradayweg 4–6, Berlin D-14195, Germany
Prof. A. Y. Cao
Department of Advanced Materials and Nanotechnology
College of Engineering
Peking University
Beijing 100871, P.R. China
E-mail: anyuan@pku.edu.cn

DOI: 10.1002/adfm.201001602

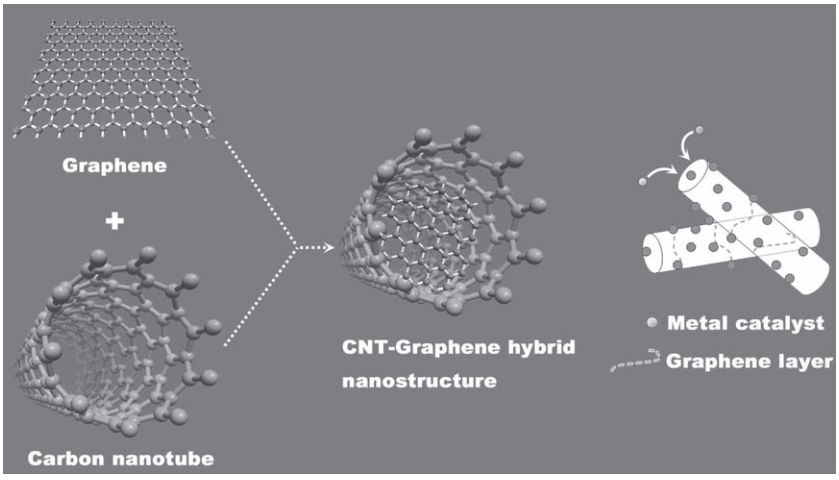

Scheme 1. Structure illustration of nitrogen-doped carbon nanotube-graphene hybrid nanostructure (NCNT-GHN) with open-ended tips. The graphene layers inside the inner cavity of the CNTs can afford additional anchoring points for metal catalyst nanoparticles in virtue of the open-ended tips of CNTs. Moreover. the graphene layers can serve as additional electron transport pathways inside the CNTs, which is beneficial to the formation of an effective three-dimensional conductive network between different NCNT-GHNs.

for immobilization of metal nanoparticles.[7i,10] If open-ended NCNTs with graphene layers distributed inside their inner cavities could be obtained, a novel support with improved performance can be expected. In this hierarchical NCNT-graphene hybrid nanostructure (NCNT-GHN), the simultaneous utilization of both the external and internal space of the NCNTs would be possible as the catalyst particles would also access the graphene layers via the open-ended tips, as shown in **Scheme 1**. Moreover, because graphene behaves as a completely transparent contact with the CNTs,[11] the graphene layers could serve as additional electron transport pathways inside the CNTs, which would be beneficial to the formation of an effective three-dimensional (3D) conductive network between the different NCNT-GHNs. More electron transport pathways via a 3D conductive network formed by NCNT-GHNs are expected to result in an enhanced electrocatalytic activity of noble metal catalysts. However, to the best of our knowledge, there are no reports about this novel nanostructure up to now.

In this work, open-ended NCNT-GHNs with graphene layers grown in situ inside the large inner cavities (ca. 50 nm) of the NCNTs were synthesized by a one-step water-assisted chemical vapor deposition (CVD) route. By using PtRu as the model catalyst, we synthesized well-dispersed PtRu nanoparticles immobilized onto the NCNT-GHN support (PtRu/NCNT-GHN) for application as high-performance methanol electrooxidation (MEO) catalyst. Furthermore, in order to evaluate their practical electrocatalytic performance, a direct methanol fuel cell (DMFC) based on PtRu/NCNT-GHN was assembled, which exhibited a much higher cell voltage, enhanced power density, and better long-term stability than those of DMFCs based on conventional PtRu/CNT and commercial MEO catalysts.

2. Results and Discussion

The synthesis of NCNT-GHNs was achieved by a water-assisted CVD process, details of which can be found in the Experimental section. The morphology of the as-synthesized NCNT-GHN is shown in **Figure 1**. Scanning electron microscopy (SEM) characterization of the as-grown NCNT-GHNs reveals their carpet-like, well-aligned, and open-ended morphology (Figure 1a–d). Furthermore, the CNT products are free of amorphous impurities, which can be attributed to the efficient in situ removal of amorphous carbon by the water vapor during the growth of the CNTs.[12] The transmission electron microscopy (TEM) images reveal a bamboo-like structure of the individual CNTs with large inner diameters (ca. 50 nm), and in particular, many thin membranes consisting of around 1–5 graphene layers formed in situ in the inner cavities of the CNTs (Figure 1e–h). These graphene membranes were initially grown as part of the CNT walls, and then detached from the wall at different positions with different number of layers (Figure 1h). This indicates a typical two-level hierarchical nanostructure that is different to other micro-sized-nanosized carbon structures.[13] In this case, 2D graphene membranes are distributed inside the inner cavities of quasi 1D CNTs. The graphene layers can serve as additional electron-transport pathways and immobilization sites for metal nanoparticles inside open-ended CNTs. The formation of this interesting open-ended NCNT-GHN structure may be attributed to the comprehensive contribution of water-assistance, the nitrogen-containing precursor, and optimum CVD growth conditions. Figure S1 shows a typical TEM image of the NCNT product grown without water assistance, which has a "cup-shaped" morphology with thick carbon layers inside the inner cavities of the nanotube. Previous work from our group[12b,12d] and others[12a,c] have proven that water vapor can act as both a catalyst promoter during nanotube growth, as well as a weak oxidant to etch the nanotube walls or tips, which is favorable for the growth of thin-walled and open-ended CNTs. In this work, the formation of graphene layers inside the CNT inner cavities might also be attributed to the etching effect of water vapor during growth.

To confirm the N doping in the NCNT-GHN structure, X-ray photoelectron spectroscopy (XPS) measurements were carried out, which showed a predominant narrow graphitic C 1s peak at 284.6 eV along with a N 1s peak at around 400.8 eV (**Figure 2**a). The high-resolution XPS N 1s spectrum given in the inset of Figure 2a reveals the presence of both pyridine-like (398.6 eV) and pyrrolic-like (400.8 eV) nitrogen atoms,[14] both of which play important roles in the electrocatalytic process.[15] The peak at 402.6 eV may be assigned to oxidized nitrogen, similar to the case of nitrogen-doped single-walled carbon nanotubes.[16] Moreover, electrochemical impedance spectra (EIS) were used to evaluate the electric conductive performance. Conventional multi-walled CNTs and carbon black (CB) were also characterized for comparison. As illustrated in Figure 2b, all of them show combinations of depressed semicircles at high- and mid-frequencies and straight-line features in the low-frequency region. Interpretation of the EIS was based on the equivalent circuit shown in the inset of Figure 2b, where C_d, Z_w, R_{ct}, and R_s denote the capacitance

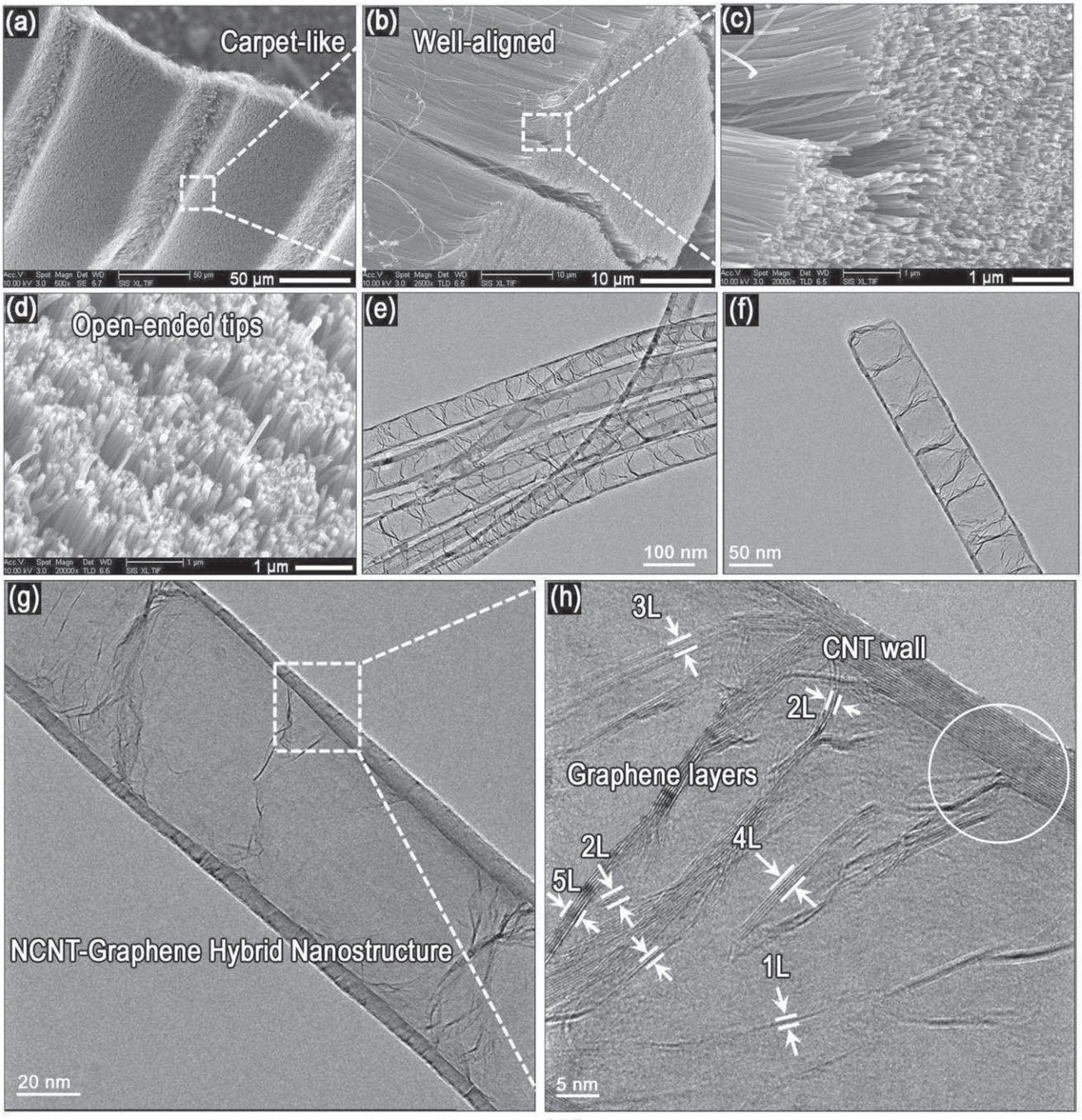

Figure 1. Morphology of the as-synthesized N-doped CNT–graphene hybrid nanostructure (NCNT-GHN). a–d) SEM images at different magnifications, which indicate that the as-obtained NCNT-GHN is carpet-like, highly pure, well-aligned, and open-ended in nature; e-g) TEM images with different magnifications; h) HRTEM image of NCNT-GHN, which shows that 1–5 graphene layers derived from the inner walls of CNTs, as pointed out in the circle part.

of the double layer, Warburg impedance, charge-transfer resistance, and solution resistance, respectively. The high-frequency semicircle in the EIS is attributed to the solid electrolyte interface (SEI) film and contact resistance,[17] and the mid-frequency semicircle to the R_{ct} on the electrode/electrolyte interface. The onset decrease point of the semicircle is usually attributed to the total electric resistance of the electrode materials, electrolyte resistance, and electric leads.[18] Thus, based on Figure 2b, the total electric resistance of the NCNT-GHN sample is 11.6 Ohm, which is remarkably lower than those of the CB sample (28.0 Ohm) and CNT sample (17.1 Ohm). This might be attributed to the contribution of graphene layers inside NCNT cavities.

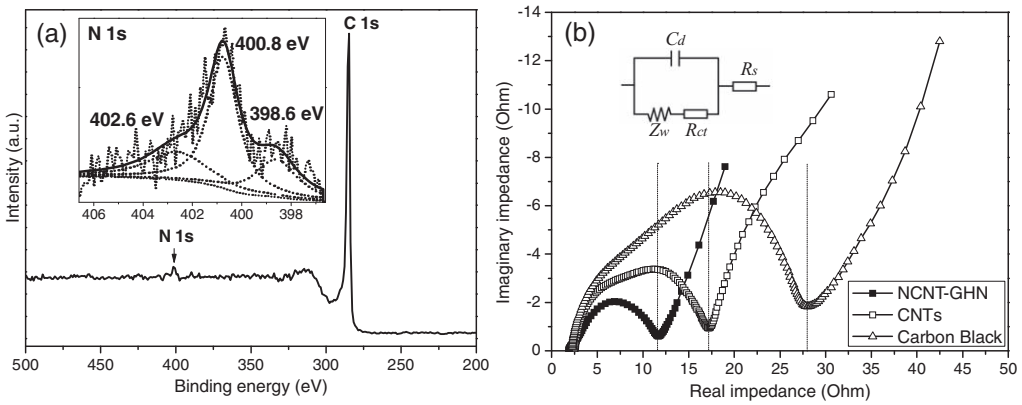

Figure 2. a) XPS spectra of the NCNT-GHN sample. The inset of (a) shows a high-resolution N 1s spectrum, which can be split into three Lorentzian peaks at 402.6, 400.8, and 398.6 eV. b) Electrochemical impedance spectra (EIS) of NCNT-GHN, conventional multi-walled CNTs, and carbon black. The inset of (b) shows the equivalent circuit.

As is well known, graphene exhibits extremely high, room-temperature carrier mobilities of around 10 000 $cm^2\ V^{-1}\ s^{-1}$,[19] which might aid in decreasing the electric resistance of the NCNT-GHN support by forming 3D electronic conductive networks, as illustrated in Scheme 1.

The 3D hierarchical structure and highly conductive networks indicated that NCNT-GHN is promising as an ideal electrocatalyst support material by facilitating fast electron transfer in many redox reactions. In order to load noble metal nanoparticles in a well-controlled way, we developed a low-temperature (ice bath) chemical reduction (LTCR) route for loading monodispersed PtRu nanoparticles onto CNT-based supports. Compared to a conventional impregnation method,[20] microemulsion method,[21] atomic layer deposition,[22] or polyol method,[23] the LTCR method is relatively simple and efficient for the fabrication of well-dispersed metal nanoparticles. Details are summarized in the Experimental section. Here, we loaded PtRu (40 wt%) nanoparticles onto NCNT-GHN by the LTCR method. As a control sample, conventional CNTs without N-doping and inner graphene sheets were also loaded with PtRu particles at the same weight percentage through the same process (**Figure 3**a). As shown in Figure S2, X-ray diffraction (XRD) patterns of as-synthesized PtRu/NCNT-GHN and PtRu/CNT catalysts both display the characteristic peaks of Pt face-centered cubic (fcc) diffraction, except that all 2θ values are shifted to slightly higher values. This indicates that a PtRu solid solution is formed at the atomic level with a basically unaltered fcc structure. The average PtRu particle size estimated from the (220) peak according to the Scherrer equation is 2.8 nm, which is close to that of particles prepared by the polyol method (2.9 nm).[23b] Figure 3 shows the TEM images of PtRu/CNT (Figure 3a) and PtRu/NCNT-GHN (Figure 3b–d). It can be seen that the PtRu nanoparticles are well-dispersed on the NCNT-GHN support materials though no pretreatment (e.g., acid treatment, polymer wrapping, etc.) steps were used. The PtRu particle size is in the range of 2–4 nm, which is close to the value estimated from XRD analysis. However, in the case of a CNT support without pretreatment, it is seen that the PtRu nanoparticles easily form aggregates, as pointed out by the circles in Figure 3a. The reason for obtaining well-dispersed PtRu nanoparticles on our NCNT-GHN support can be understood by the enhanced noble metal anchoring through the activation of nitrogen-neighboring carbon atoms because of the large electron affinity of nitrogen, as was proven by theoretical calculations.[9] Especially, in the case of our PtRu/NCNT-GHN catalysts, it is possible that the PtRu nanoparticles access the inner space of the CNTs and graphene layers from their open ends, as shown in Figure 3c–d.

Thermogravimetric analysis (TGA) and differential thermal analysis (DTA) curves demonstrate the difference between the oxidation behavior of the PtRu/NCNT-GHN and PtRu/CNT samples, as shown in **Figure 4**a. In the temperature ranges of 100–500 °C and 700–1000 °C, both PtRu/NCNT-GHN and PtRu/CNT samples show similar trends. However, in the range of 500–700 °C, the weight losses show a different behavior, which can be attributed to the differences in the PtRu nanoparticle size and dispersion between these two samples. Because noble metal nanoparticles are generally oxidized in air atmosphere at high temperatures, which leads to a weight gain, the quick weight loss caused by carbon combustion is hampered. Consequently, an inflection point occurred at around 500 °C for both catalysts. However, because of the quantum-size effect, the smaller and well-dispersed PtRu nanoparticles will be oxidized at a faster rate and thus lead to an overall weight gain. Meanwhile, as demonstrated by the TEM results in Figure 3, the PtRu nanoparticles in the PtRu/NCNT-GHN catalyst have a smaller average size and better dispersion than those in the PtRu/CNT catalyst. Therefore, as the overall weight gain is caused by the quicker PtRu oxidation reaction and this is faster for smaller particles, the weight percentage of PtRu/NCNT-GHN is higher than that of PtRu/CNT at each temperature in the range of 500–700 °C, as shown in Figure 4a.

The methanol oxidation electrocatalytic activities of the as-obtained catalysts were evaluated by cyclic voltammetry (CV) (Figure 4b). Two commercial MEO catalysts, Pt(40 wt%)/carbon black from Johnson Matthey Co. (denoted as Pt/C (JM)) and PtRu(40 wt%)/carbon black from E-TEK Co. (Pt/Ru = 1:1 atomic ratios, denoted as PtRu/C (E-TEK)), were also used for comparison. It can be seen from Figure 4b and Table S1 that the oxidation peak current density in the forward sweep for PtRu/NCNT-GHN is about 500.5 mA mg^{-1}, which is almost 2.5 times of PtRu/C (E-TEK) (203.9 mA mg^{-1}) and 3.3

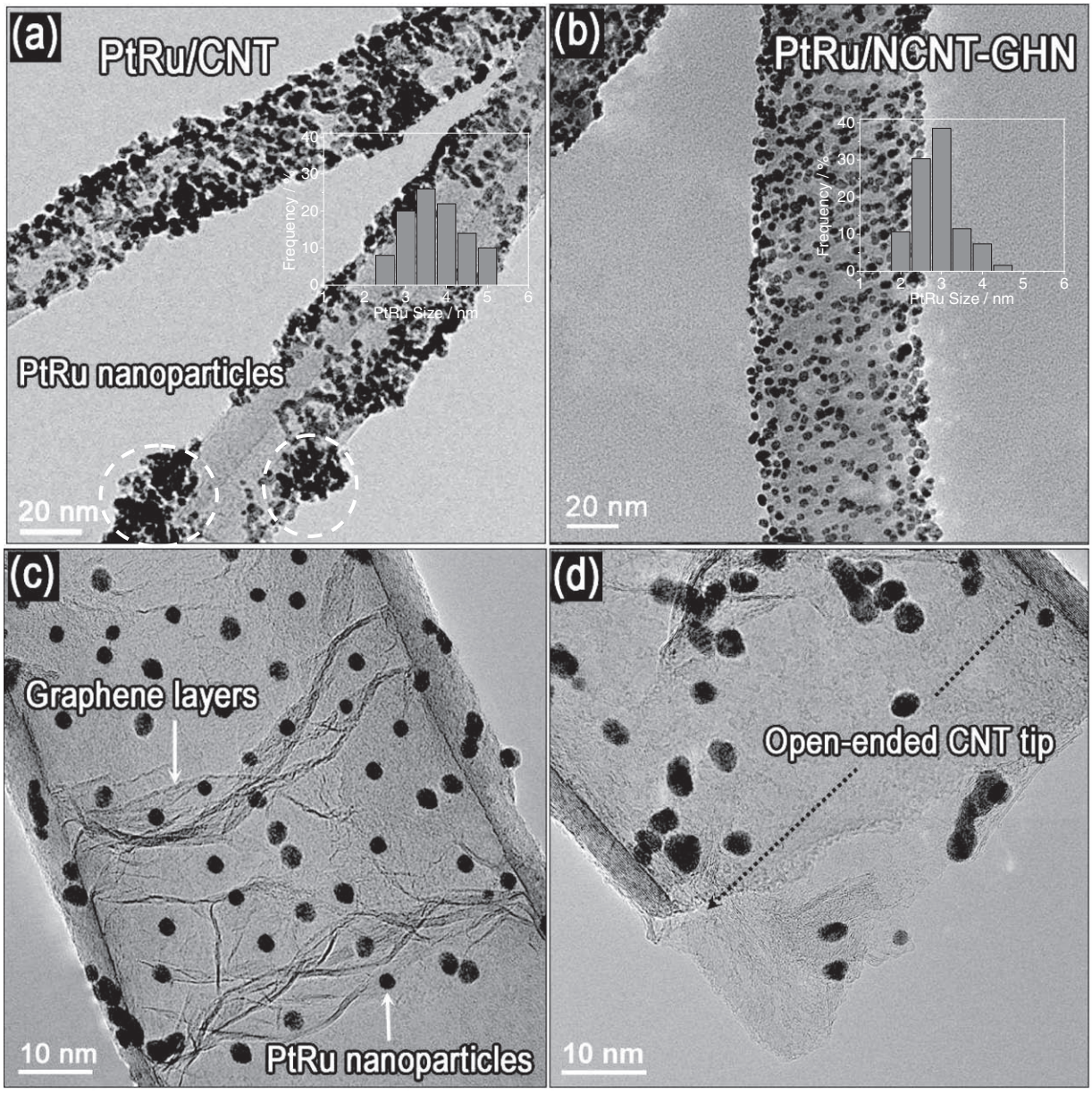

Figure 3. Morphology of PtRu nanoparticles loaded onto different CNTs by using a low-temperature chemical reduction (LTCR) method. a) PtRu nanoparticles on conventional multi-walled CNTs, where it can be seen that the PtRu nanoparticles easily form aggregates, as pointed out by the circles. b–d) well-dispersed PtRu nanoparticles on NCNT-GHN. Graphene layers inside the NCNTs can afford additional anchoring positions for PtRu nanoparticles, in virtue of the open-ended tip structure of the NCNTs. The insets in (a) and (b) are the corresponding size-distribution histograms of the PtRu nanoparticles in the PtRu/CNT and PtRu/NCNT-GHN samples.

times of Pt/C (JM) (152.8 mA mg^{-1}) catalysts. After nitrogen-doping and introduction of graphene layers inside the inner cavities, the PtRu/NCNT-GHN catalyst shows a higher MEO activity than that of the PtRu/CNT catalyst (399.5 mA mg^{-1}). The enhancement of methanol oxidation can be attributed to the following two aspects. On the one hand, the incorporation of nitrogen influences the chemical reactivity and electronic conductivity of the CNTs by changing their electronic structures,[7i,24] and thus is promotional to the effective immobilization of noble-metal nanoparticles by strengthening the metal-support interactions. On the other hand, graphene layers inside the NCNTs can afford additional anchoring points for the metal nanoparticles, and are also favorable to the construction of a 3D electric conductive network between the different NCNT-GHNs. Thus, the breaking of C-H bonds and subsequent removal of the CO_{ads}-like intermediates by oxidation with OH_{ads} species supplied by Ru-OH sites tend to be performed at a relatively low onset potential. Consequently, as indicated in Figure 4b and Table S1, the onset potential of the PtRu/NCNT-GHN catalyst is lower than that of the PtRu/CNT and commercial PtRu/C (E-TEK) catalysts, but a little higher than that of Pt/C (JM).

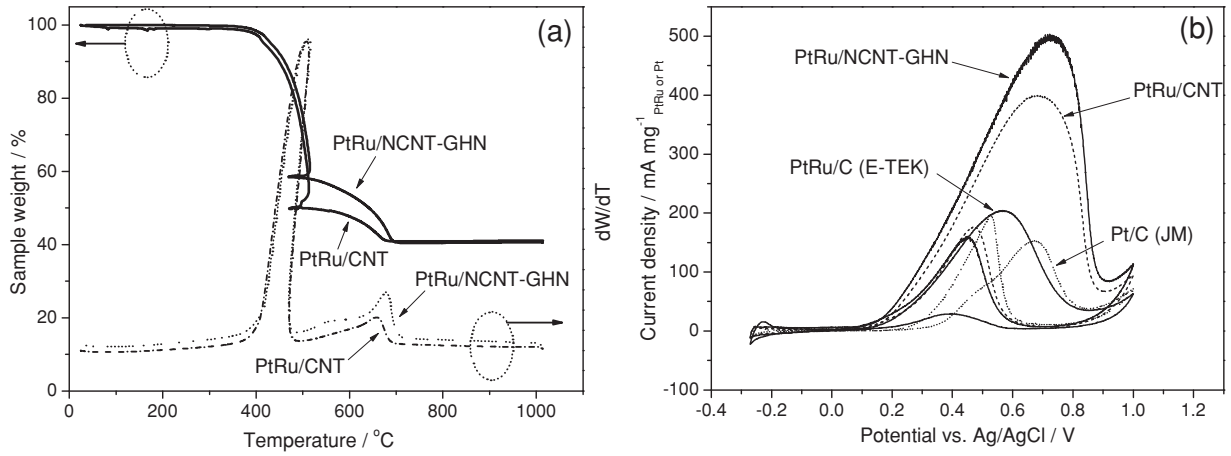

Figure 4. a) TG/DTA curves of two as-synthesized catalysts measured in air atmosphere at a heating rate of 10 °C min^{-1} from ambient temperature to 1000 °C. b) cyclic voltammograms of different catalysts in N_2-saturated 1.0 mol L^{-1} methanol + 0.5 mol L^{-1} H_2SO_4 at a scanning rate of 10 mV s^{-1}.

DMFC single cells were assembled for testing the electrocatalytic performance of PtRu/NCNT-GHN. **Figure 5** shows the dependence of voltage and power density on current density recorded at different temperatures of 30, 60, and 90 °C. It can be seen from Figure 5a–c that, when the working temperature increases from 30 to 90 °C, both the output voltage and power density rise accordingly. In the case of the PtRu/NCNT-GHN catalyst, peak power densities are observed at 195.3, 546.9, and 781.3 mA cm^{-2} at 30, 60, and 90 °C, respectively. As shown in Table S2, these values are much higher than

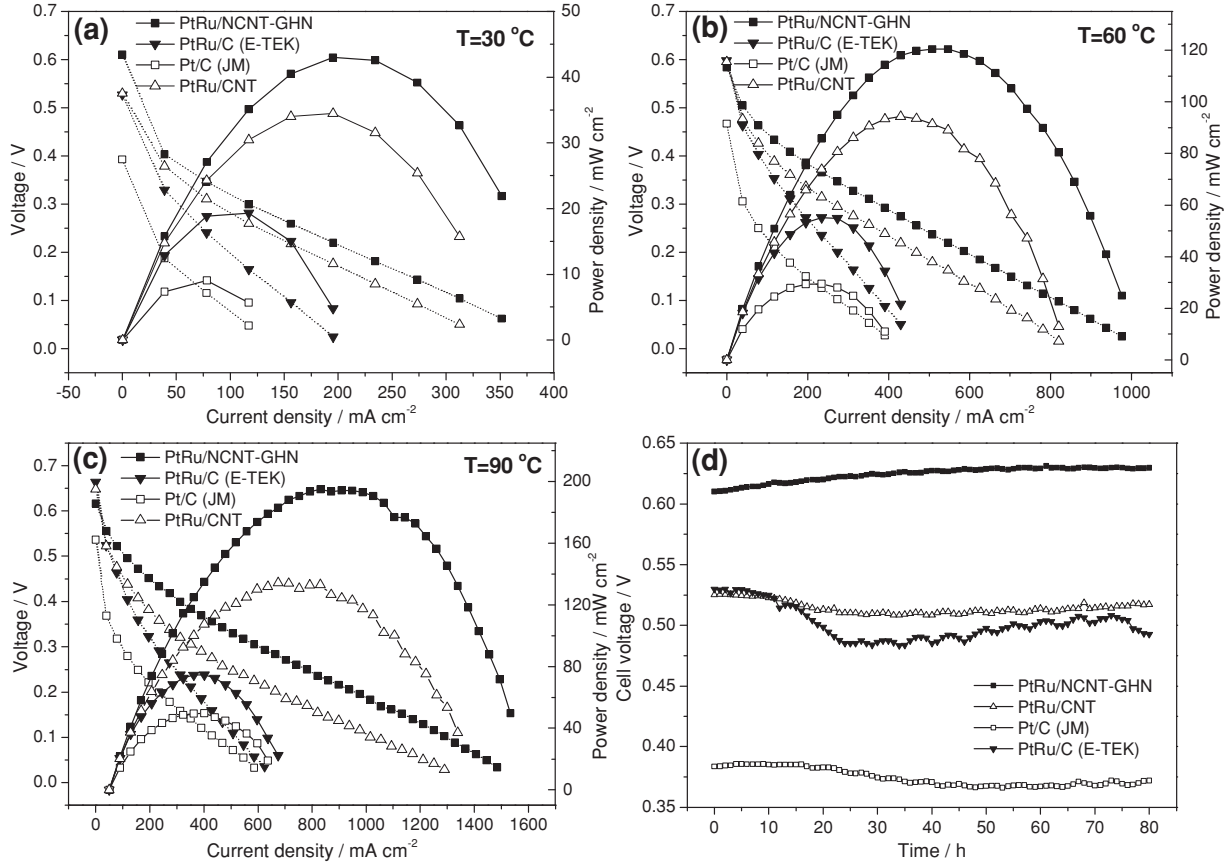

Figure 5. DMFC single-cell properties of different catalysts at a) 30, b) 60, and c) 90 °C. d) Durability test of DMFC single cells with different MEO catalysts at 30 °C using 2 mol L^{-1} methanol solution. It can be seen that the as-synthesized PtRu/NCNT-GHN catalyst demonstrates good stability at a higher output voltage than other MEO catalysts.

those of commercial catalysts, and also higher than those of PtRu/CNT, which are 156.3, 429.7 and 664.1 mA cm^{-2} at 30, 60, and 90 °C, respectively. The maximum power densities on various catalysts are illustrated in Figure S3. These results are in good agreement with their MEO activities revealed by CV measurements, confirming the synergy enhancement through their hierarchical structure and N doping. From Figure 5a and Figure S3, it can be seen that the maximum power densities of the as-synthesized PtRu/NCNT-GHN catalyst at 30 °C is about 43.0 mA cm^{-2}, which also demonstrates advantages over that of PtRu/PCNF (PCNF denotes platelet-type carbon nanofibers) prepared by a microwave-polyol method (33.5 mA cm^{-2}).[23b] In addition, the durability of our PtRu/NCNT-GHN catalyst in long-term operation was evaluated. Figure 5d shows a galvanostatic curve of DMFC single cells with different MEO catalysts. The PtRu/NCNT-GHN single cell demonstrates a much better long-term operation stability compared to the PtRu/CNT and commercial MEO catalysts from Johnson Matthey and E-TEK. Furthermore, the cell voltage of PtRu/NCNT-GHN (>0.6 V) was much higher than that of PtRu/CNT and the two commercial catalysts (<0.55 V) at the same operating temperature. The reason for this may be that because of the lone electron pair on the sp^2 orbital at the nitrogen site (e.g., pyridinic site) in the plane of carbon rings NCNT-GHN immobilizes the PtRu nanoparticles more firmly and better dispersed, and thus the catalyst particles that are grafted on NCNT-GHNs have a higher stability and enhanced activity in methanol oxidation.

3. Conclusions

High-purity, open-ended, and well-aligned NCNT-GHNs were synthesized by a water-assisted CVD route and used as highly efficient support materials for noble metal (PtRu) nanoparticles. A synergistic enhancement of the electronic structure (N-doping) and hierarchical structure (graphene-CNT hybrid) is demonstrated during the MEO process. On the one hand, the incorporation of nitrogen is promotional to the effective immobilization of noble metal nanoparticles by strengthening the metal-support interaction. On the other hand, graphene layers inside the NCNTs can afford additional anchoring points for metal nanoparticles, and are also favorable to the construction of a 3D electric conductive network between different NCNT-GHNs. The as-synthesized PtRu/NCNT-GHN catalyst shows an improved electrocatalytic performance and better long-term operation stability for methanol electrooxidation than both a prepared PtRu/CNT catalyst and commercial MEO catalysts. Based on this novel NCNT-graphene hybrid nanostructure, many other interesting applications might also be discovered in areas such as heterogeneous catalysis, gas storage, energy-conversion and -storage applications, etc.

4. Experimental Section

Synthesis of NCNT-GHNs: The experimental setup and procedure were similar to that described in our previous report on NCNTs,[25] however, here, a low concentration of water vapor was introduced into the CVD reactor during NCNT growth. In a typical run, ferrocene powder was dissolved in acetonitrile to form a solution with a concentration of 20 mg mL^{-1}, and fed into the CVD furnace at 860 °C by a syringe pump at a constant rate of 0.4 mL min^{-1} for 30 min. A mixture of Ar and H_2 was purged through the system at 2000 and 300 sccm, respectively. At the same time, water vapor with a dew point of -20 °C was introduced into the CVD reactor under Ar flow. A quartz slide was used to collect the products.

Low-Temperature Chemical Reduction for Loading of PtRu Nanoparticles: The synthesis of the PtRu/NCNT-GHN catalyst was performed in an ice bath. In a typical synthesis of PtRu(40 wt%)/NCNT-GNH catalyst, 1.0 g NCNT-GNH was added into 100 mL of deionized water to form a suspension by magnetic stirring. Then, aqueous solutions of $H_2PtCl_6{\cdot}6H_2O$ (1.18 g) and $RuCl_3{\cdot}2H_2O$ (0.55 g) were added dropwise and separately into the NCNT-GNH suspension. These feedstock amounts correspond to a 40 wt% PtRu/NCNT-GHN catalyst with a Pt:Ru stoichiometric atomic ratio of 1:1. $NaBH_4$ was then added into the suspension to start the reduction reaction. After the reduction was finished, the product was filtered and washed by deionized water. Finally, the product was dried in 80 °C and ground into a fine black powder for further characterization and electrochemical measurements. Conventional CNTs were also loaded with PtRu nanoparticles for comparison by using the same process.

Material Characterization: Scanning electron microscopy (SEM) images were obtained by a JEOL JSM-6700F instrument. Transmission electron microscopy (TEM) images were acquired with a JEM-2100F, using an accelerating voltage of 200 kV. XRD data were obtained using a Japan Rigaku D/max RB X-ray diffractometer equipped with graphite monochromatized high-intensity Cu Kα radiation (λ = 0.15406 nm). X-ray photoelectron spectroscopy (XPS) spectra were obtained using a PHI Quantera in a vacuum chamber of 1.4×10^{-8} Torr, and using Al Kα (1486.7 eV) laser excitation. Electrochemical impedance spectroscopy (EIS) was recorded using an IM6ex (Zahner) electrochemical workstation. The details of the EIS measurements can be found in our previous work.[26] Thermogravimetric analysis (TGA) was carried out from ambient temperature to 1000 °C in air flow at a heating rate of 10 °C min^{-1}.

Cyclic Voltammetry: The half-cell electrochemical tests were performed in a three-electrode system at room temperature. To prepare the working electrode, 0.1 g of the PtRu/NCNT-GHN (or another catalyst, such as PtRu/CNT) sample was dispersed in 0.5 g H_2O + 0.5 g Nafion solution (5 wt%, Wako), and then magnetically stirred for 12 h to form a uniform slurry. Then 10 μL of the slurry was dropped onto a gold electrode (10.02 mm in diameter) to form a uniform catalyst layer and then dried at 60 °C for 15 min. A platinum foil and Ag/AgCl electrode were used as the counter electrode and the reference electrode, respectively.

DMFC Single-Cell Performance Tests: For a membrane electrode assembly (MEA) used in the DMFC (Figure S4(a)), an anode prepared from PtRu/NCNT-GHN (or another catalyst, e.g., PtRu/CNT) and a cathode prepared from Pt black (7 mg cm^{-2}; Johnson Matthey Co.) were formed on Teflon-coated carbon paper substrates using catalyst inks containing the appropriate weight percentage of Nafion solution (5 wt%, Wako). The MEA for single-cell tests was fabricated by hot-pressing as-prepared cathode and anode layers onto both sides of a pretreated Nafion 117 electrolyte membrane at 165 °C under a pressure of 4 MPa for 10 min. Single-cell performances were evaluated in a DMFC unit cell with a 2.5 cm × 2.5 cm cross-sectional area (Figure S4(b)) and measured with an fuel cell impedance meter (KIKUSUI, KFM2030, Japan). Both fuel and oxidant flow paths were machined into graphite block end-plates, which also served as current collectors. A methanol solution (2 mol L^{-1}) with a flow rate of 2.0 mL min^{-1} and dry O_2 with 200 sccm flow were supplied to the anode and cathode, respectively. The optimum methanol concentration (2 mol L^{-1}) was determined by both the DMFC performance contrast at different methanol concentrations (Figure S5) and previous literature.[7b,c,23a,27] Single-cell tests were carried out at 30 °C, 60 °C, and 90 °C. The durability of the MEAs with different anode catalysts was tested in corresponding DMFC single cells.

Supporting Information

Supporting Information is available from the Wiley Online Library or from the author.

Acknowledgements

The authors are grateful for the financial support from the National Natural Science Foundation of China (Grant No. 50902080, 50632040), the China Postdoctoral Science Foundation (Grant No. 20090450021), and from the Guangdong Province Innovation R&D Plan. We also appreciate the kind help from Dr. Lin Gan and Dr. Hongda Du (Tsinghua University) in fruitful discussions.

Received: August 3, 2010
Revised: November 3, 2010
Published online: February 2, 2011

[1] a) S. H. Joo, S. J. Choi, I. Oh, J. Kwak, Z. Liu, O. Terasaki, R. Ryoo, *Nature* **2001**, *412*, 169; b) S. Alayoglu, A. U. Nilekar, M. Mavrikakis, B. Eichhorn, *Nat. Mater.* **2008**, *7*, 333; c) J. Zhang, H. Z. Yang, J. Y. Fang, S. Z. Zou, *Nano Lett.* **2010**, *10*, 638.

[2] G. R. Li, F. Wang, Q. W. Jiang, X. P. Gao, P. W. Shen, *Angew. Chem. Int. Ed.* **2010**, *49*, 3653.

[3] a) E. Castillejos, P. J. Debouttiere, L. Roiban, A. Solhy, V. Martinez, Y. Kihn, O. Ersen, K. Philippot, B. Chaudret, P. Serp, *Angew. Chem. Int. Ed.* **2009**, *48*, 2529; b) Y. H. Ng, S. Ikeda, T. Harada, S. Higashida, T. Sakata, H. Mori, M. Matsumura, *Adv. Mater.* **2007**, *19*, 597; c) S. Ikeda, S. Ishino, T. Harada, N. Okamoto, T. Sakata, H. Mori, S. Kuwabata, T. Torimoto, M. Matsumura, *Angew. Chem. Int. Ed.* **2006**, *45*, 7063.

[4] S. H. Sun, C. B. Murray, D. Weller, L. Folks, A. Moser, *Science* **2000**, *287*, 1989.

[5] H. A. Gasteiger, S. S. Kocha, B. Sompalli, F. T. Wagner, *Appl. Catal. B-Environ.* **2005**, *56*, 9.

[6] E. Antolini, *Appl. Catal. B-Environ.* **2009**, *88*, 1.

[7] a) A. Halder, S. Sharma, M. S. Hegde, N. Ravishankar, *J. Phys. Chem. C* **2009**, *113*, 1466; b) Z. M. Cui, C. P. Liu, J. H. Liao, W. Xing, *Electrochim. Acta* **2008**, *53*, 7807; c) J. Prabhuram, T. S. Zhao, Z. K. Tang, R. Chen, Z. X. Liang, *J. Phys. Chem. B* **2006**, *110*, 5245; d) S. J. Guo, S. J. Dong, E. K. Wang, *Adv. Mater.* **2010**, *22*, 1269; e) H. Chu, Y. Shen, L. Lin, X. Qin, G. Feng, Z. Lin, J. Wang, H. Liu, Y. Li, *Adv. Funct. Mater.* **2010**, *20*, 3747; f) B. H. Wu, D. Hu, Y. J. Kuang, B. Liu, X. H. Zhang, J. H. Chen, *Angew. Chem. Int. Ed.* **2009**, *48*, 4751; g) M. Okamoto, T. Fujigaya, N. Nakashima, *Small* **2009**, *5*, 735; h) D. Wang, Z. C. Li, L. W. Chen, *J. Am. Chem. Soc.* **2006**, *128*, 15078; i) R. Chetty, S. Kundu, W. Xia, M. Bron, W. Schuhmann, V. Chirila, W. Brandl, T. Reinecke, M. Muhler, *Electrochim. Acta* **2009**, *54*, 4208.

[8] J. P. Tessonnier, D. Rosenthal, F. Girgsdies, J. Amadou, D. Begin, C. Pham-Huu, D. S. Su, R. Schlogl, *Chem. Commun.* **2009**, 7158.

[9] Y. H. Li, T. H. Hung, C. W. Chen, *Carbon* **2009**, *47*, 850.

[10] H. Y. Du, C. H. Wang, H. C. Hsu, S. T. Chang, U. S. Chen, S. C. Yen, L. C. Chen, H. C. Shih, K. H. Chen, *Diamond Relat. Mater.* **2008**, *17*, 535.

[11] A. L. Elias, A. R. Botello-Mendez, D. Meneses-Rodriguez, V. J. Gonzalez, D. Ramirez-Gonzalez, L. Ci, E. Munoz-Sandoval, P. M. Ajayan, H. Terrones, M. Terrones, *Nano Lett.* **2010**, *10*, 366.

[12] a) L. Ci, S. M. Manikoth, X. Li, R. Vajtai, P. M. Ajayan, *Adv. Mater.* **2007**, *19*, 3300; b) R. T. Lv, F. Y. Kang, W. X. Wang, J. Q. Wei, X. F. Zhang, Z. H. Huang, J. L. Gu, K. L. Wang, D. H. Wu, *Phys. Status Solidi A-Appl. Mater.* **2007**, *204*, 867; c) K. Hata, D. N. Futaba, K. Mizuno, T. Namai, M. Yumura, S. Iijima, *Science* **2004**, *306*, 1362; d) A. Cao, X. Zhang, C. Xu, J. Liang, D. Wu, B. Wei, *J. Mater. Res.* **2001**, *16*, 3107.

[13] a) Z. B. Zhao, J. Y. Qu, J. S. Qiu, X. Z. Wang, Z. Y. Wang, *Chem. Commun.* **2006**, 594; b) D. S. Su, X. W. Chen, G. Weinberg, A. Klein-Hofmann, O. Timpe, S. B. A. Hamid, R. Schlogl, *Angew. Chem. Int. Ed.* **2005**, *44*, 5488; c) M. Q. Zhao, Q. Zhang, X. L. Jia, J. Q. Huang, Y. H. Zhang, F. Wei, *Adv. Funct. Mater.* **2010**, *20*, 677; d) Q. Zhang, M. Q. Zhao, Y. Liu, A. Y. Cao, W. Z. Qian, Y. F. Lu, F. Wei, *Adv. Mater.* **2009**, *21*, 2876.

[14] R. Arrigo, M. Havecker, R. Schlogl, D. S. Su, *Chem. Commun.* **2008**, 4891.

[15] K. P. Gong, F. Du, Z. H. Xia, M. Durstock, L. M. Dai, *Science* **2009**, *323*, 760.

[16] F. Xu, M. Minniti, P. Barone, A. Sindona, A. Bonanno, A. Oliva, *Carbon* **2008**, *46*, 1489.

[17] K. Fukuda, K. Kikuya, K. Isono, M. Yoshio, *J. Power Sources* **1997**, *69*, 165.

[18] a) C. Y. Lee, H. M. Tsai, H. J. Chuang, S. Y. Li, P. Lin, T. Y. Tseng, *J. Electrochem. Soc.* **2005**, *152*, A716; b) Y. K. Zhou, B. L. He, W. J. Zhou, H. L. Li, *J. Electrochem. Soc.* **2004**, *151*, A1052.

[19] a) A. K. Geim, *Science* **2009**, *324*, 1530; b) K. S. Novoselov, A. K. Geim, S. V. Morozov, D. Jiang, Y. Zhang, S. V. Dubonos, I. V. Grigorieva, A. A. Firsov, *Science* **2004**, *306*, 666.

[20] a) J. C. Kang, S. L. Zhang, Q. H. Zhang, Y. Wang, *Angew. Chem. Int. Ed.* **2009**, *48*, 2565; b) F. B. Su, J. H. Zeng, X. Y. Bao, Y. S. Yu, J. Y. Lee, X. S. Zhao, *Chem. Mater.* **2005**, *17*, 3960; c) V. Raghuveer, A. Manthiram, *J. Electrochem. Soc.* **2005**, *152*, A1504.

[21] M. Kim, S. Hwang, J. S. Yu, *J. Mater. Chem.* **2007**, *17*, 1656.

[22] C. Liu, C. C. Wang, C. C. Kei, Y. C. Hsueh, T. P. Perng, *Small* **2009**, *5*, 1535.

[23] a) L. Gan, R. T. Lv, H. D. Du, B. H. Li, F. Y. Kang, *Electrochem. Commun.* **2009**, *11*, 355; b) M. Tsuji, M. Kubokawa, R. Yano, N. Miyamae, T. Tsuji, M. S. Jun, S. Hong, S. Lim, S. H. Yoon, I. Mochida, *Langmuir* **2007**, *23*, 387.

[24] Y. Y. Shao, J. H. Sui, G. P. Yin, Y. Z. Gao, *Appl. Catal. B-Environ.* **2008**, *79*, 89.

[25] T. Cui, R. Lv, F. Kang, Q. Hu, J. Gu, K. Wang, D. Wu, *Nanoscale Res. Lett.* **2010**, *5*, 941.

[26] R. Lv, L. Zou, X. Gui, F. Kang, Y. Zhu, H. Zhu, J. Wei, J. Gu, K. Wang, D. Wu, *Chem. Commun.* **2008**, *17*, 2046.

[27] a) J. B. Ge, H. T. Liu, *J. Power Sources* **2005**, *142*, 56; b) H. Dohle, J. Divisek, R. Jung, *J. Power Sources* **2000**, *86*, 469; c) T. Yuan, Z. Q. Zou, M. Chen, Z. L. Li, B. J. Xia, H. Yang, *J. Power Sources* **2009**, *192*, 423.